Comparative Medicine
Copyright 2008
by the American Association for Laboratory Animal Science

Vol 58, No 6
December 2008
Pages 542–550

Quantitative Tomography of Early-Onset Spontaneous AA Amyloidosis in Interleukin 6 Transgenic Mice

Jonathan S Wall,[1,*] Tina Richey,[1] Amy Allen, Robert Donnell,[2] Steve J Kennel,[1] and Alan Solomon[1]

Mice that constitutively express the human interleukin 6 (huIL6) protein from a heritable transgene (*H2-L^d-IL-6*) express high levels of the acute-phase reactant, serum amyloid protein A, a liver-derived apoprotein of high-density lipoprotein that is the precursor of AA amyloid. Typically at approximately 5 mo of age B6(C)- *Tg(H2-L^d-IL-6)Kish* (H2/huIL-6) animals begin to develop splenic deposits of AA amyloid, which progress to involve the liver, kidney, and vasculature, ultimately resulting in death due to severe systemic AA amyloidosis at 8 to 9 mo of age. These mice provide a robust model in which to study novel therapeutic and diagnostic imaging agents for AA amyloidosis. We recently have noted a change in onset of spontaneous disease, as evidenced by 2 female transgenic mice that were found moribund at only 5 mo of age. Extensive hepatosplenic amyloid deposits in both mice were identified and quantified by single-photon emission computed tomography, which further revealed heterogeneous distribution of radiotracer in the spleen indicating a distinction between amyloid-laden red pulp and the disease-free lymphoid follicles. The AA nature of the deposits was evidenced immunohistochemically and by mass spectrometric analyses of extracted amyloid fibrils. Our studies have documented the manifestation of early-onset, severe, spontaneous AA amyloidosis in 2- to 5-mo-old H2/huIL-6 mice; we hypothesize that this disease is due to genetic rather than environmental factors.

Abbreviations: au, arbitrary units; CT, computed tomography; huIL6, human interleukin 6; SAP, serum amyloid P; SPECT, single photon emission computed tomography; sAA, serum amyloid A.

AA amyloidosis is the most common form of systemic amyloid disease in animals, occurring in cheetah,[5,36] shar-pei dogs,[8,11] sheep,[10,34] goats,[34] ducks,[13] cats,[45,46] hamsters,[20,35] dolphins,[7] common marmosets[30] and, especially, mice.[2,4,15,20] Typically, this disorder results from overproduction of an acute-phase reactant termed serum amyloid protein A (sAA), the amyloidogenic precursor protein, which is synthesized almost exclusively by hepatocytes.[3,26,33,39] Serum amyloid protein A binds heparan sulfate proteoglycan and laminin within the basement membrane and modulates cholesterol metabolism.[29,37,44]

For more than 50 y mice have been used as an experimental model for AA, whereby animals are injected with a proinflammatory stimulus, such as silver nitrate, casein solution, Freund adjuvant, or lipopolysaccharide to generate an acute-phase response.[15] Variations of this experimental model are used to study the etiology of amyloidosis and for the discovery and testing of novel therapies.[22,25,47] One drawback, however, is the need to provide repeated chemical injections, with attendant toxicity, to maintain the pathology. Cessation of the inflammatory stimulus results in slow but progressive resorption of the amyloid deposits.[25]

As an alternative approach, we characterized and maintained a line of mice that express the human IL6 (huIL6) protein from a stably inserted transgene. The B6(C)- *Tg(H2-L^d-IL-6)Kish* (H2/huIL-6) strain was derived at the National Institutes of Health by introgressive backcrossing of the original H2-L^d-IL-6 Tg C57BL/6 transgenic mice[42,43] onto the Balb/c background for more than 20 generations.[28] These mice constitutively express the huIL6 transgene under the control of the mouse major histocompatibility complex class 1 (H2-L^d) promoter. The transgene segregates with an autosomal pattern of Mendelian inheritance.[43] Because of the role of IL6 in maintenance of the inflammatory response and lymphocyte proliferation during the immune response, early generations of these transgenic animals had high sAA levels and an extensive lymphocytosis with development of polyclonal plasma cell proliferation in 56% of mice at 18 mo of age.[28]

Human IL6 serum levels in the early generations of this transgenic line were 0.5 to 1 ng/mL[43]; however, backcrossed Balb/c mice bred in our facility for approximately 2 y had approximately 300-fold higher with circulating huIL6 levels at 8 wk of age (0.3 to 1 µg/mL).[41] In response to the proinflammatory huIL6 cytokine, the mice experience a chronic inflammatory state that results in increased concentrations of circulating sAA-conjugated high-density lipoprotein. The spontaneous onset of AA amyloidosis in these mice typically occurred at age 5 mo, presenting first as perifollicular deposits in the spleen only detectable histologically by biopsy.[41] Over the course of the next 3 to 4 mo, amyloid was detected in the periportal vasculature and sinusoids within the liver, tongue, heart and intestinal villi, as well as renal interstitium, glomerulae, and papilla. In addition, cast nephropathy was commonly observed, as was extramedullary hematopoiesis and

Received: 16 Feb 2008. Revision requested: 18 Apr 2008. Accepted: 24 Jun 2008.
[1]Human Immunology and Cancer Program, Graduate School of Medicine, and [2]Department of Pathobiology, College of Veterinary Medicine, University of Tennessee, Knoxville, TN.
[*]Corresponding author. Email: jwall@mc.utmck.edu

splenomegaly due to amyloidosis or lymphoid hyperplasia (or both) resulting from the elevated IL6 concentrations.

We previously documented the nature of the amyloid in H2/huIL-6 mice immunohistochemically by using AA-specific monoclonal antibodies.[41] In addition, we used liquid chromatography-coupled mass spectrometry to show that isolated tissue-derived AA fibrils were comprised of a truncated form of sAA containing the first 77 N-terminal amino acids (residues 1 to 77).[41] No evidence of apolipoproteins AI and AII or immunoglobulin light chain has been found during immunohistochemical examination and liquid chromatography-coupled mass spectrometry of the amyloid extracted from these mice. In addition, the organ distribution of the disease was visualized through whole-body single-photon emission computed tomography (SPECT imaging) by using the amyloidophilic protein serum amyloid P component (SAP) as a tracer;[17,18,48,49] however, quantitative analysis of AA deposition from high-resolution ('single-pinhole') SPECT data was not possible.

Recently, we have noted that several of our H2/huIL-6 mice exhibited a phenotype indicative of severe amyloidosis at as early as 3 to 5 mo of age. Here we present imaging-based case studies of 2 kindred animals that became moribund at approximately 5 mo of age. SPECT images for which iodinated SAP was used as a tracer revealed hepatosplenic AA amyloid deposits, which were quantified by using a novel image-based approach and were of sufficiently high resolution to discriminate the amyloid-laden red pulp from the amyloid-free lymphoid follicles of the spleen.

Materials and Methods

Animals. All animal procedures were performed under the auspices of protocols approved by the University of Tennessee Animal Care and Use Committee; the University of Tennessee is an AAALAC-accredited institution. The health status of the entire colony is assessed every 3 mo, when serum samples from sentinel mice are evaluated (Comprehensive Serology Profile For Mice, Research Animal Diagnostic Laboratory, Columbia, MO). For the past 5 y, each test on this profile has been negative, indicating the healthy status of the colony. H2/huIL-6 transgenic mice on a Balb/c background initially were provided by Dr Michael Potter[28] in 1997. Animals were housed 4 per cage under conventional conditions in microisolation caging with nonirradiated corncob bedding (Harlan Teklad, Madison, WI). The mice were fed a standard diet (25/5 Rodent Diet, Harlan Teklad) and had access to water and food ad libitum. The line was maintained by using both IL6 × IL6 and IL6 × wild-type matings. At 3 to 4 wk after birth, pups were weaned and a tail section harvested for genotyping by using huIL6-specfic primers, as previously described.[41] The 2- to 5-mo-old kindred female H2/huIL-6 mice described here were found displaying a 'hunched' resting posture, failure to groom adequately, and abnormally low levels of inquisitive behavior.

SPECT and CT imaging. Human SAP, isolated from human pleural fluid by affinity chromatography (a gift of Professor Philip Hawkins, Royal Free Hospital, London, UK), was radioiodinated with ^{125}I (Perkin Elmer, Waltham, MA) by using a low concentration of chloramine T sufficient to protect the protein from the effects of excessive and damaging oxidation.[49] The radiolabeled product was purified by gel filtration and its radiochemical purity established by SDS-PAGE and analyzed by phosphoimaging (Cyclone Storage Phosphor System, Perkin Elmer). Mice were injected with 300 µCi (approximately 25 µg) of ^{125}I-SAP diluted in PBS containing 5 mg/mL bovine serum albumin in the lateral tail vein and then housed in a satellite facility, with food and water provided ad libitum for 24 h under a 12:12-h light:dark cycle, after which they were given an intravenous injection of vascular CT contrast agent (200 µL; Fenestra VC, Advanced Research Technologies, Quebec, CA) and euthanized 15 min later by isoflurane inhalation overdose by using the drop chamber method.

SPECT and CT images were acquired by using a microCAT II + SPECT imaging platform (Siemens Preclinical Solutions, Knoxville, TN). Mice were positioned prone on a cardboard platform and the board placed on the scanner bed. To facilitate post hoc coregistration of the CT and SPECT images, three 70-µCi ^{57}Co point sources secured to the underside of the animal support served as fiducial markers. The CT data were acquired by using X-ray voltage biased to 80 kVp with a 500-µA anode current, the full field of view was used, and the data were binned 4 × 4. An exposure of 310 msec was used, and 360 1° projections were collected. The data were reconstructed in real-time by using an implementation of the Feldkamp filtered back-projection algorithm onto a $512 \times 512 \times 768$ matrix with isotropic 0.077-mm voxels.[14]

The initial SPECT images were collected by using a 2-mm-diameter pinhole collimator positioned 36 mm from the center of the field of view. Each dataset comprised 45 projections with a 60-s exposure at each azimuth. A total number of 1.42×10^6 events were acquired by each detector. Data from a single SPECT detector were reconstructed post hoc onto a $52 \times 52 \times 68$ matrix by using a 3D ordered subset expectation maximization algorithm with 8 iterations and 4 subsets. For high-resolution SPECT, a second image was acquired by using a 0.5 mm-diameter pinhole collimator; 60 projections each with a 700-s exposure time were acquired to attain 1.78×10^6 events.

SPECT/CT image analysis. CT and SPECT datasets were imported into a 3D visualization software package (Amira, Mercury Computer Systems, Chelmsford, MA). The SPECT data were resampled onto a matrix with dimensions of $104 \times 104 \times 136$ voxels (voxel size, 0.45 mm^3) and coregistered with the CT data. The spleen and liver volumes were segmented manually from the SPECT images and the volume, mean intensity per voxel, and total organ intensity (an indirect measure of the amyloid content) determined. All images were rendered by using the same visualization parameters in the Amira program.

Biodistribution of ^{125}I-SAP in the mice. Samples of spleen, pancreas, kidney, liver, heart, and lung tissue were harvested from both mice after euthanasia. Each sample was placed into a tared plastic vial and weighed, and the I-125 radioactivity was measured by using an automated Wizard 3 gamma counter (1480 Wallac Gamma Counter, Perkin Elmer, Waltham, MA). The biodistribution data were expressed as percentage of injected dose per gram of tissue (% ID/g). In addition, samples of each tissue were fixed in 10% buffered formalin for 24 h and embedded in paraffin for histology and autoradiography.

Autoradiography and histology. For autoradiography, 4- to 6-µm thick sections were cut from formalin-fixed, paraffin-embedded blocks onto Plus microscope slides (Fisher Scientific, Pittsburgh, PA), dipped in NTB2 emulsion (Eastman Kodak, Rochester, NY), stored in the dark, and developed after a 96-h exposure.[49] Each section was counterstained with hematoxylin. Tissue amyloid deposits were identified microscopically in consecutive tissue

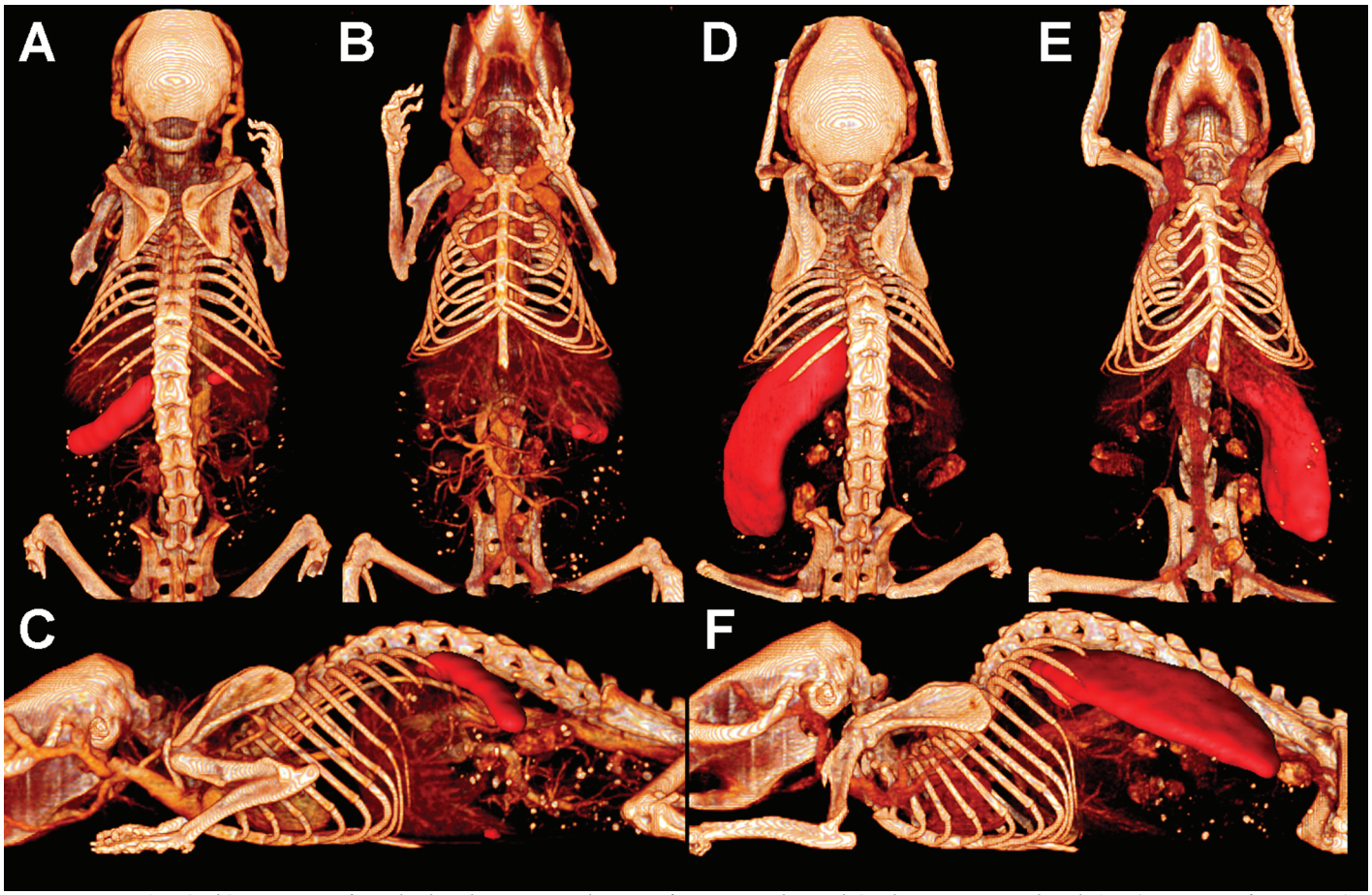

Figure 1. MicroSPECT/CT imaging of amyloid. Volumetric renderings of contrast-enhanced CT data coregistered with SPECT images of mouse 1 (A, dorsal; B, ventral; C, lateral) and mouse 2 (D, dorsal; E, ventral; F, lateral). ^{125}I-SAP distribution in SPECT images is false-colored red. Images were scaled to mask the lowest 25% of activity, which contains noise and streak artifacts.

sections viewed under cross-polarized illumination after staining with alkaline Congo red.[48] For immunostaining, slides were incubated in citrate antigen-retrieval solution (BioGenex, San Ramon, CA) at 90 °C for 30 min, and then an AA-reactive rabbit polyclonal antibody (provided by Dr Mark Kindy, Medical University of South Carolina) was added at a dilution of 1:45,000. The slides were developed by using the biotinylated goat antirabbit secondary antibody provided in the IHC DAB kit (InnoGenex, San Ramon, CA). All tissue sections were examined by light microscopy (DM500, Leica, Bannockburn, IL) fitted with cross-polarizing filters (for the detection of Congo red birefringence). Digital microscopic images were acquired by using a cooled charge-coupled device camera (SPOT, Diagnostic Instruments, Sterling Heights, MI).

Identification of amyloid by ion-trap mass spectrometry after antigen-retrieval. Formalin-fixed 4-µm thick sections of spleen tissue mounted on Plus slides underwent antigen retrieval by heating at 90 °C in Glyca solution (pH 4; Biogenex) for 30 min and then were dehydrated by immersion in 100% ethanol for 30 min. The tissue was scraped from the slide into a 1.5-ml microfuge tube and after complete dehydration was reduced by addition of 50 µL 100 mM DTT (Sigma, St Louis, MO) for 30 min at room temperature. The sample was alkylated by adding 50 µL 100 mM iodoacetamide (Sigma), followed by incubation in the dark at room temperature for a further 30 min. The samples were dehydrated serially with 200 µL acetonitrile, rehydrated by addition of 200 µL 100 mM ammonium bicarbonate, and finally dehydrated twice more with 200 µL acetonitrile. The tissue then was dried completely by using a vacuum concentrator (SpeedVac, Savant/Thermo Instruments, Farmingdale, NY).

Prior to mass spectrometric analysis, the samples were trypsinized by the addition of 30 µL 0.02 µg/µL trypsin (Promega, Madison, WI) for 18 h at 37 °C. After concentrating to a volume less than 20 µL by using the vacuum concentrator, the peptides were identified by directing the sample into the ion-trap mass spectrometer (LCQ Deca XP, ThermoFinnigan, San Jose, CA). The ion data were analyzed by using the Xcalibur and Sequest software packages (ThermoFinnigan).

Results

MicroSPECT/CT imaging. Two kindred female H2/huIL-6 mice were studied because they appeared moribund at 5 mo of age and showed a hunched resting posture, a phenotype usually associated with severe systemic pathology in this amyloid-prone strain of mice. To ascertain the presence and distribution of amyloidosis, small-animal SPECT/CT imaging was used to visualize the distribution of the ^{125}I-labeled SAP 24 h after intravenous injection.

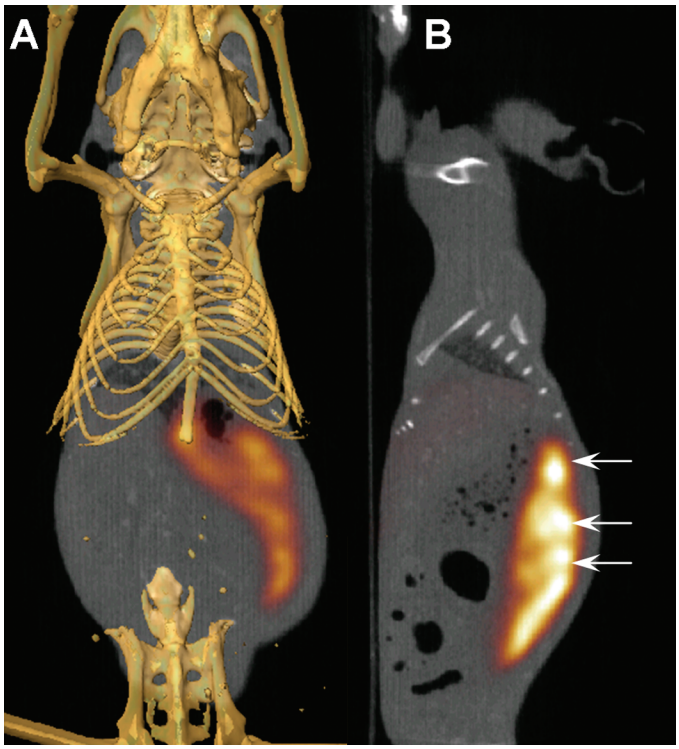

Figure 2. Heterogeneous distribution of ^{125}I-SAP in spleen of mouse 2. (A) Ventral and (B) lateral views of ^{125}I-SAP (false-colored red) in spleen shown in coregistered SPECT/CT images.

Prior to being euthanized, the mice received a bolus of vascular CT contrast medium to provide increased anatomic detail. In mouse 1, the SPECT images revealed marked accumulation of radiolabeled SAP in the spleen and, to a lesser degree, the liver (Figure 1, A through C). The spleen appeared normal in size, with apparently uniform distribution of ^{125}I-SAP along its length. In contrast, mouse 2 had a markedly enlarged spleen that spanned the entire abdominal cavity and that bound ^{125}I-SAP, indicating the presence of amyloid as well as splenomegaly (Figure 1, D through F). In images that had been scaled to reveal only the most intense 75% of SPECT activity (Figure 1), no SAP accumulation was discerned in any other organ or tissue in either mouse.

After acquiring SPECT images by using a 2-mm-diameter pinhole collimator, which afforded high sensitivity but relatively low resolution, we noted slight heterogeneity in the distribution of the ^{125}I-SAP within the spleen of mouse 2, suggesting that discrete 'pockets' of amyloid were visible. To investigate this possibility further, we acquired high-resolution SPECT images of mouse 2 by using a 0.5-mm-diameter pinhole collimator with extended image acquisition time. Analysis of these SPECT images confirmed heterogeneous distribution of radioiodinated SAP within the spleen. Planar views through the length of the spleen clearly indicated distinct foci of high activity (arrows in Figure 2), as well as of low or no activity, which were presumed to be areas that were devoid of amyloid.

Biodistribution of ^{125}I-SAP. Quantitation of the ^{125}I-SAP organ uptake (that is, % ID/g tissue) was achieved by measuring the amount of activity associated with the spleen, pancreas, kidney, liver, heart, and lungs (Figure 3). Consistent with the imaging results, the spleen and liver of both mice contained high levels

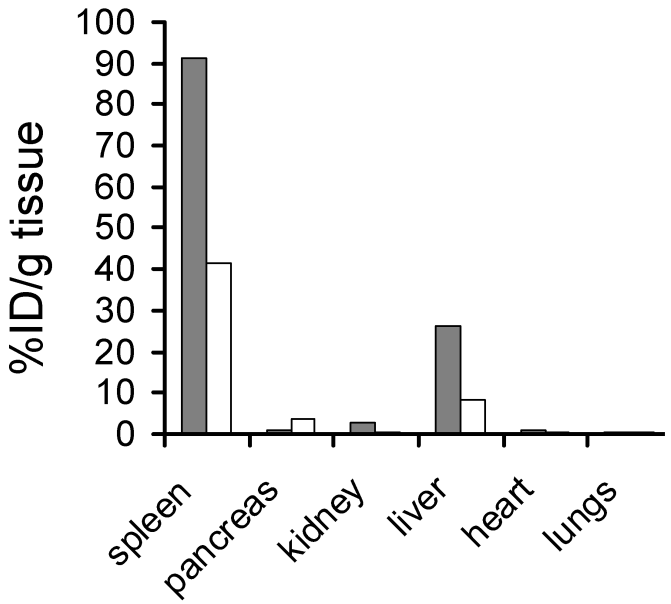

Figure 3. Biodistribution of ^{125}I-SAP. Organ-specific activity expressed as percentage of injected dose per gram of tissue (%ID/g) measured in mouse 1 (gray) and 2 (white).

of radioactivity (mouse 1: spleen, 91.3% ID/g; liver, 26.4% ID/g; mouse 2: spleen, 41.5% ID/g; liver, 8.2% ID/g). The greater accumulation of ^{125}I-SAP in the spleen relative to the liver is characteristic of the progression of amyloidosis in these mice, in which the perifollicular splenic deposits precede those observed in the vasculature and parenchyma of the liver.[1,24] In addition, mice 1 and 2 also showed uptake of radiolabeled SAP in kidneys and pancreas, respectively.

Histopathology. Deposits of amyloid, characterized by Congophilic, pale amorphous to finely fibrillar eosinophilic material that exhibited typical apple green birefringence on polarization were noted in the liver (Figure 4). The deposits were responsible for mild to moderate irregular thickening of the vascular walls and expanded the stromal extracellular matrix of the portal triads and lobular vessels. Occasional scattered deposits of amyloid were observed in walls of centrolobular veins, with rare deposition along the hepatic sinusoids (within the space of Disse). The amount of hepatic amyloid appeared more pronounced in the tissue sections from mouse 1 than in those from mouse 2.

In the spleen, the extracellular matrix of the reticular fiber network of the splenic sinusoids was markedly expanded by Congophilic amyloid that distorted the normal splenic architecture and widely separated the trabeculae and periarteriolar lymphoid sheaths. Amyloid caused irregular thickening of the arterial and venous walls within the trabeculae. The cellular population of the mildly hyperplastic lymphoid sheaths was predominantly composed of plasma cells surrounding limited populations of lymphocytes. The degree of splenic amyloid deposition was more pronounced in the sections from mouse 2 than those from mouse 1.

Microautoradiography and immunohistochemistry. The intraorgan distribution of ^{125}I-SAP in both mice was visualized by microautoradiography, as evidenced by the appearance of dark silver grains within sections of formalin-fixed, paraffin-embedded tissue after exposure to photographic emulsion (Figure 4). This technique was

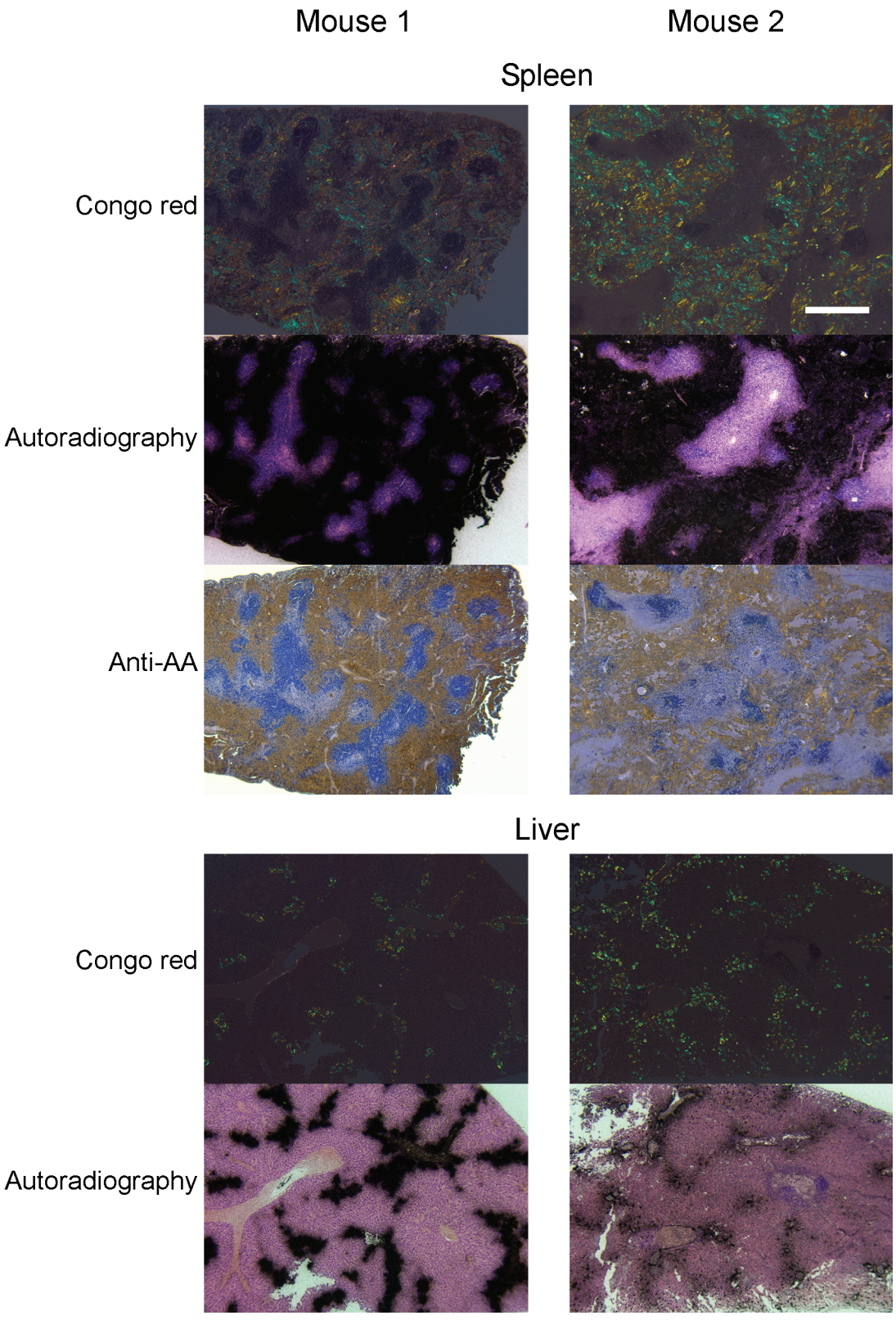

Figure 4. Colocalization of ^{125}I-SAP with AA amyloid. Distribution of ^{125}I-SAP in microautoradiographs of liver and spleen sections from mice 1 and 2 which were stained with Congo red and an anti-AA antibody.

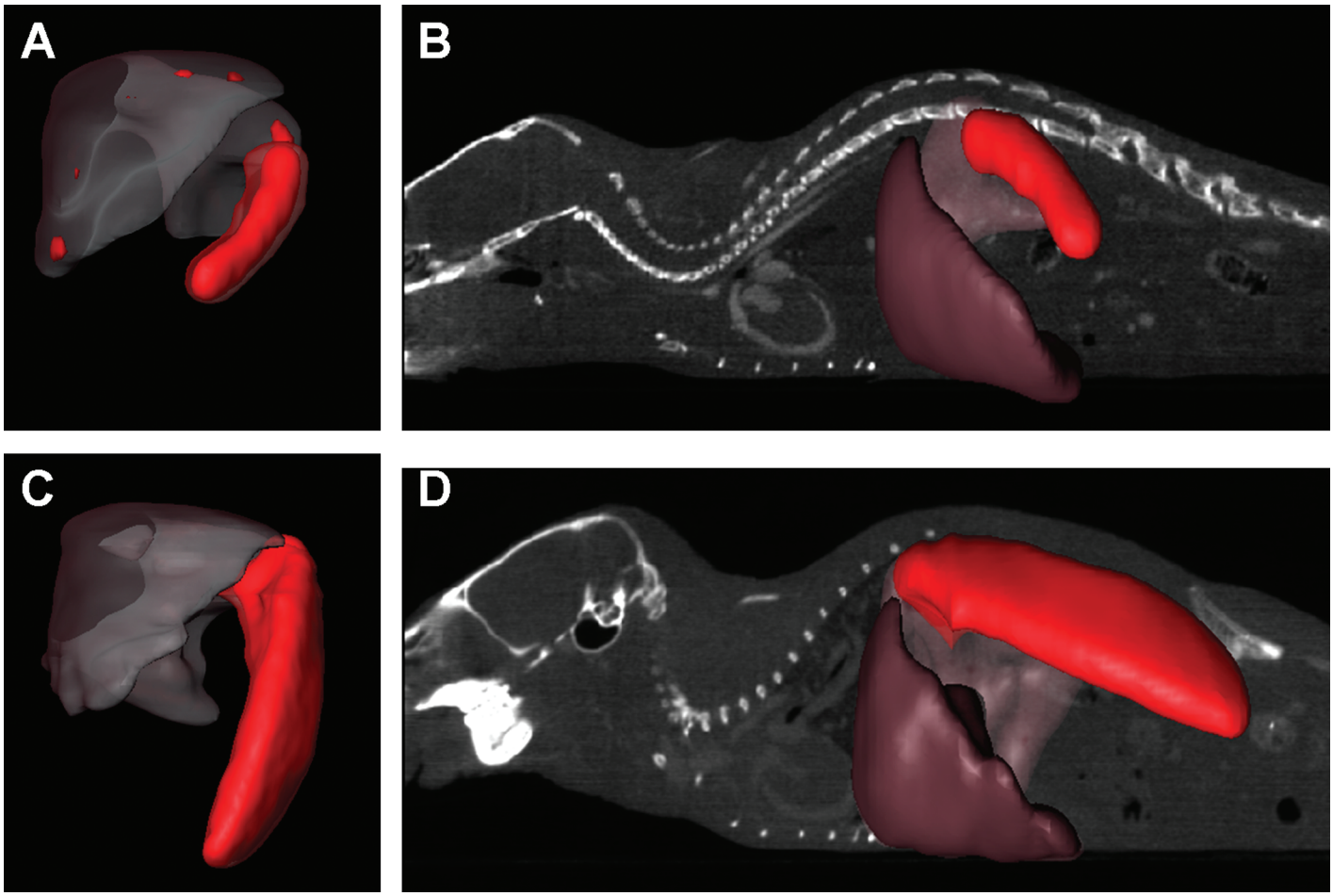

Figure 5. Organ segmentation and quantification of amyloid from SPECT images. The liver and spleen volumes were segmented from SPECT images of mouse 1 (A, B) and mouse 2 (C, D) and registered with the distribution of ^{125}I-SAP (false-colored red). (A, C) Isolated organ volumes. (B, D) Volumes coregistered with a planar CT view.

used to confirm the colocalization of ^{125}I-SAP within the hepatic and splenic Congo red-birefringent amyloid deposits that immunostained with a specific antiAA monoclonal antibody.

In the case of mouse 2, radioiodinated SAP was readily taken up by the extensive amyloid deposits that expanded the splenic red pulp. In contrast, the lymphoid follicles were remarkably devoid of both amyloid and ^{125}I-SAP, as evidenced both by autoradiography and histochemistry (Figure 4). The liver of mouse 2 contained scant perivascular amyloid deposits that infiltrated the sinusoids. In both mice, the distribution of the Congophilic amyloid correlated with that of the ^{125}I-SAP, indicating the specificity of this tracer for fibrils.

Quantification of amyloid by SPECT. We previously demonstrated that SPECT can be used to provide a semiquantitative measure of organ amyloid content based on the correlation between radioiodinated SAP uptake and the amount of amyloid determined by the extent of Congo red birefringence.[48] This method complements the biodistribution determined by counting tissue samples; indeed the image-based method provides less-biased quantification because no tissue sampling is required. The liver and spleen data were selected from the SPECT image data by manually selecting those voxels that were anatomically associated with each organ and for which the signal strength was greater than background (that is, >10% of total signal). The resulting 3D volumes for the 2 organs are shown in Figure 5. In the case of mouse 1, the liver measured 1269.6 mm^3 and the liver was 155.1 mm^3 (Table 1). The mean voxel intensity in the SPECT images, which provides a measure of the concentration of ^{125}I-SAP per unit volume and therefore amyloid density, was 2-fold greater for the spleen than the liver. For mouse 2, the spleen was approximately 4.5 times the volume of that calculated for mouse 1, consistent with the marked splenomegaly in mouse 2. The liver of mouse 2 was slightly enlarged, with a volume 34% greater than that of mouse 1 (Table 1). Because the intensity of each voxel in the SPECT image was, to a first approximation, directly proportional to the concentration of ^{125}I-SAP in that anatomical site and, therefore, the amount of amyloid, the segmented data could be used to determine a quantitative measure of the amyloid burden in each organ. This analysis revealed that the spleen in mouse 2 and the liver in mouse 1 contained the greatest quantities of amyloid; these amyloid burdens were approximately equivalent between the mice, that is, 4×10^6 arbitrary units (au).

Mass spectrometric analysis of AA. Confirmation that the amyloid in the organs of both mice was indeed AA in nature was obtained through liquid chromatography–mass spectroscopy of fibrils extracted from the animals' spleens (Table 2). The 4 AA-

Table 1. Amyloid burden in liver and spleen established from SPECT images

	Volume (mm^3)[a]	Mean voxel intensity (au)	Amyloid burden index (au × 10^6)[b]
Mouse 1			
Liver	1269.6	311.2	4.2
Spleen	155.1	537.9	0.89
Mouse 2			
Liver	1705.0	95.3	1.7
Spleen	677.7	611.6	4.4

[a]The segmented volume based on activity in the SPECT image [number of voxels × voxel volume (0.091 mm^3)].
[b]Total ^{125}I-SAP-associated SPECT activity in organ [mean voxel intensity (au) × voxel number].

Table 2. Identification of mouse AA peptides by mass spectrometry

AA sequence	Peptide	Mass	z	x_{corr}[a]	ΔCn[b]	Ions[c]
18–25	RAYTDMKE	728.8	1	1.16	0.25	6/10
39–47	RGNYDAAQRG	894.9	1	1.03	0.17	6/14
46–57	RGPGGVWAAEKI	972.1	2	3.16	0.61	16/18
61–71	RESFQEFFGRG	1147.2	2	3.10	0.38	14/16

[a]The fit of the observed product in the spectrum versus the theoretical spectra created from available database sequences.
[b]Delta correlation, score between the top 2 candidate peptide matches (significant if value is > 0.2).
[c]The number of peptide fragment ions matched/total number of expected fragment ions.

related peptides contained more than 35% of the 103 amino acids of murine sAA, with the N-terminal fragment of amino acids 1 to 77 identified as the primary component.

Pedigree of Mice To establish a possible genetic cause, we examined a 6-generation pedigree (Figure 6) that included mouse 1 (no. 1405) and 2 (no. 1410) as well as other H2/huIL-6 mice that have since been either found dead or moribund at 4 or 5 mo of age and for whom amyloidosis had been diagnosed from Congo red-stained tissue smears. Both mice 1 and 2 were derived from a mating that also gave rise to lineages that resulted in early-onset AA amyloidosis and premature morbidity, thereby implying that genetic factors (such as increased transgene copy number[6]) rather than environmental factors (such as exogenous sources of AEF[34,40]) likely were responsible for this phenomenon.

Discussion

We previously reported that severe systemic AA amyloidosis occurs in H2/huIL-6 mice at 8 mo of age.[41] However, recently we observed a hunched posture and moribund state in mice as young as 3 to 5 mo of age. Spontaneous pathologies in mice that express a huIL6 transgene include progressive renal damage including cast nephropathy, plasmacytosis, lymphoma, and AA amyloidosis.[09,43] However, in general, morbidity due to IL6 overexpression or any other cause is not seen in huIL6 transgenic mice younger than 8 mo.[09,41,43] The use of H2/huIL-6 mice for drug validation or to study the etiopathology of amyloidosis requires them to be amyloid-free at 2 mo of age so that initiation of the disease can be investigated—something that could not be achieved in mice with early-onset AA. Therefore, we sought to confirm the nature of the amyloid pathology and investigate the mechanisms responsible for the early disease onset.

MicroSPECT imaging using ^{125}I-SAP as an amyloid-specific radiotracer demonstrated the presence of AA amyloid deposits in the spleen (and, to a much lesser degree, in the liver) of both mice. The volumes of the livers in both mice, calculated by using the SPECT images, were in good agreement with other published values determined from magnetic resonance imaging (1.53 cm^3)[27] and from estimations based on organ mass using a density of 1.06 g/cm.[35] In contrast, the calculated volume of the spleens in mice 1 and 2 were 2- and 10-fold greater, respectively, than that reported for a 25-g mouse.[27] We considered that the extreme splenomegaly in mouse 2 was due to both extensive amyloid deposition that expanded the reticular sinusoidal network of the red pulp as well as to follicular lymphoid hyperplasia and plasmacytosis. This combination resulted in a macroscopic heterogeneous pattern of ^{125}I-SAP distribution that was visible in the SPECT images. In mouse 2, the amyloid-free follicles could be discerned from the amyloid-laden red pulp particularly well in the high-resolution SPECT images acquired with the 0.5-mm pinhole collimator. Our previous analyses had not revealed these intraorgan anatomic details in H2/huIL-6 mice with AA amyloidosis.

We thought it likely that the absolute amount of amyloid burden led to the early morbidity in the H2/huIL-6 mice. Previously we reported ^{125}I-SAP doses as high as 20% ID/g in the spleen of H2/huIL-6 mice (either induced by using amyloid-enhancing factor or in mice older than 8 mo).[48] The mice with early-onset AA amyloidosis had 2- to 4-fold greater amounts of amyloid than did H2/huIL-6 mice 8 wk after injection of AEF.[48] Therefore, not only did spontaneous AA occur earlier in the mice we present here but the amount of amyloid deposited was greater than that observed previously in AEF-induced H2/huIL-6 mice. We therefore took this opportunity to define a new measurement of amyloid burden based on the SPECT images.

The amyloid burden index expresses the product of the organ volume by the mean organ voxel intensity in the SPECT image (which correlates with the concentration of ^{125}I-SAP accumulation and, by extension, the amount of amyloid). This value provides a measure of the total amyloid content of an organ and therefore differs from the value of "mean voxel intensity per unit volume," which we have used previously.[48] Consequently, the current analysis demonstrated that although the spleen appeared in the SPECT images to be the major site of amyloid deposition, the liver

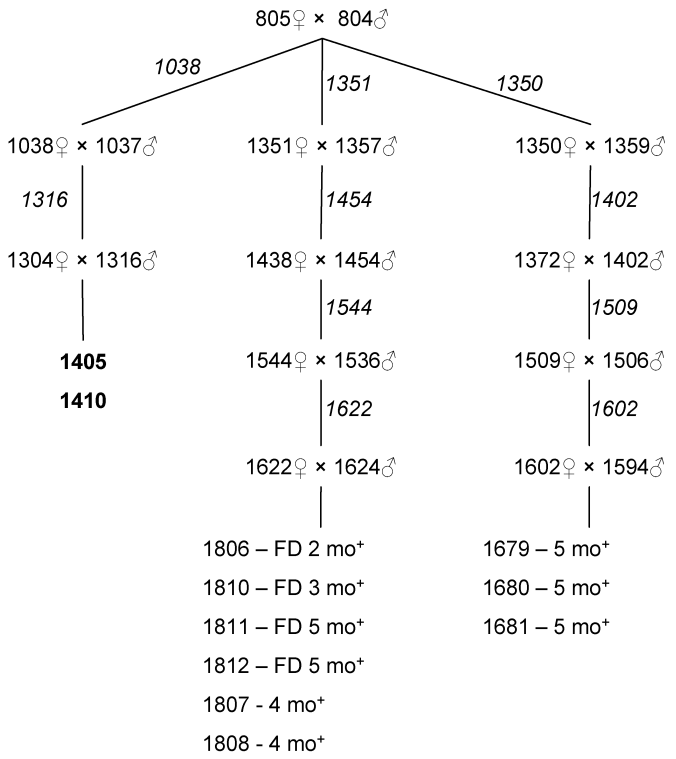

Figure 6. Six-generation pedigree for mice 1 and 2. Mouse 1 (no. 1405), mouse 2 (no. 1410), and 2 other breeding lines were derived from a single mating between mice 805 and 804. FD, found dead; +, Congo red-confirmed AA amyloidosis.

(because of its larger volume) actually contained substantially more amyloid. The relatively concentrated distribution of splenic amyloid explains why the spleen was more apparent than the liver in the SPECT images. Therefore, care must be taken to discern the difference between amyloid concentration and absolute amyloid burden—both of which can be measured from whole-body microSPECT imaging studies.

In summary, our data show that the early moribundity in the H2/huIL-6 mice was due to the early onset of AA amyloid deposition in exceptionally high amounts. AA amyloid was confirmed immunohistochemically in the 2 mice we present here, and the body burden of AA amyloid was estimated by using a novel quantitative metric derived from the microSPECT images. This technique allows differentiation of total-organ amyloid load and "amyloid concentration." This effect could be due to either genetic or epigenetic factors.

Acknowledgments

We thank Sallie Macy and Craig Wooliver for immunohistochemical and histologic tissue staining, respectively; Charles Murphy for the LC-MS analysis of amyloid extracts; and Professor Philip Hawkins for the gift of human SAP. This work was supported in part by US Public Health Service Research grant EB00789 from the National Institute of Biomedical Imaging and Bioengineering and National Institute of Neurologic Disease and Stroke. AS is an American Cancer Society Research Professor.

References

1. **Ailles L, Kisilevsky R, Young ID**. 1993. Induction of perlecan gene expression precedes amyloid formation during experimental murine AA amyloidogenesis. Lab Invest **69:**443–448.
2. **Ali-Khan Z, Li W, Chan SL.** 1996. Animal model for the pathogenesis of reactive amyloidosis. Parasitol Today **12:**297–302.
3. **Artl A, Marsche G, Lestavel S, Sattler W, Malle E.** 2000. Role of serum amyloid A during metabolism of acute-phase HDL by macrophages. Arterioscler Thromb Vasc Biol **20:**763–772.
4. **Benditt EP, Hoffman JS, Eriksen N, Parmelee DC, Walsh KA.** 1982. SAA, an apoprotein of HDL: its structure and function. Ann N Y Acad Sci **389:**183–189.
5. **Bergstrom J, Ueda M, Une Y, Sun X, Misumi S, Shoji S, Ando Y.** 2006. Analysis of amyloid fibrils in the cheetah (*Acinonyx jubatus*). Amyloid **13:**93–98.
6. **Chandler KJ, Chandler RL, Broeckelmann EM, Hou Y, Southard-Smith EM, Mortlock DP.** 2007. Relevance of BAC transgene copy number in mice: transgene copy number variation across multiple transgenic lines and correlations with transgene integrity and expression. Mamm Genome **18:**693–708.
7. **Cowan DF.** 1995. Amyloidosis in the bottlenose dolphin, *Tursiops truncatus*. Vet Pathol **32:**311–314.
8. **DiBartola SP, Tarr MJ, Webb DM, Giger U.** 1990. Familial renal amyloidosis in Chinese Shar Pei dogs. J Am Vet Med Assoc **197:**483–487.
9. **Fattori E, Della Rocca C, Costa P, Giorgio M, Dente B, Pozzi L, Ciliberto G.** 1994. Development of progressive kidney damage and myeloma kidney in interleukin-6 transgenic mice. Blood **83:**2570–2579.
10. **Fernandez A, Mensua C, Biescas E, Lujan L.** 2003. Clinicopathological features in ovine AA amyloidosis. Res Vet Sci **75:**203–208.
11. **Flatland B, Moore RR, Wolf CM, Yeomans SM, Donnell RL, Lane IF, Fry MM**. 2007. Liver aspirate from a Shar Pei dog. Vet Clin Pathol **36:**105–108.
12. **Ge F, Yao J, Fu X, Guo Z, Yan J, Zhang B, Zhang H, Tomozawa H, Miyazaki J, Sawashita J, Mori M, Higuchi K**. 2007. Amyloidosis in transgenic mice expressing murine amyloidogenic apolipoprotein AII (Apoa2c). Lab Invest **87:**633–643.
13. **Gorevic PD, Greenwald M, Frangione B, Pras M, Franklin EC.** 1977. The amino acid sequence of duck amyloid A (AA) protein. J Immunol **118:**1113–1118.
14. **Gregor J, Gleason S, Paulus MJ, Cates J.** 2002. Fast Feldkamp reconstruction based on focus of attention and distributed computing. Intl J Imaging Syst Technol **12:**229–234.
15. **Gruys E, Snel FW.** 1994. Animal models for reactive amyloidosis. Baillieres Clin Rheumatol **8:**599–611.
16. **Gruys E, Tooten PC, Kuijpers MH.** 1996. Lung, ileum, and heart are predilection sites for AApoAII amyloid deposition in CD1 Swiss mice used for toxicity studies. Pulmonary amyloid indicates AApoAII. Lab Anim **30:**28–34.
17. **Hawkins PN.** 1994. Diagnosis and monitoring of amyloidosis. Baillieres Clin Rheumatol **8:**635–659.
18. **Hawkins PN, Pepys MB.** 1995. Imaging amyloidosis with radiolabelled SAP. Eur J Nucl Med **22:**595–599.
19. **Higuchi K, Naiki H, Kitagawa K, Hosokawa M, Takeda T.** 1991. Mouse senile amyloidosis. ASSAM amyloidosis in mice presents universally as a systemic age-associated amyloidosis. Virchows Arch B Cell Pathol Incl Mol Pathol **60:**231–238.
20. **Hol PR, Snel FW, Niewold TA, Gruys E.** 1986. Amyloid-enhancing factor (AEF) in the pathogenesis of AA-amyloidosis in the hamster. Virchows Arch B Cell Pathol Incl Mol Pathol. **52:**273–281.
21. **Husby G, Husebekk A, Skogen B, Sletten K, Marhaug G, Magnus J, Syversen V.** 1988. Serum amyloid A (SAA)—the precursor of protein AA in secondary amyloidosis. Adv Exp Med Biol **243:**185–192.
22. **Inoue S, Hultin PG, Szarek WA, Kisilevsky R**. 1996. Effect of poly(vinylsulfonate) on murine AA amyloid: a high-resolution ultrastructural study. Lab Invest **74**:1081–1090.
23. **Kisilevsky R**. 2005. Preparation and propagation of amyloid-enhancing factor. Methods Mol Biol **299**:237–241.
24. **Kisilevsky R, Boudreau L**. 1983. Kinetics of amyloid deposition. I. The effects of amyloid-enhancing factor and splenectomy. Lab Invest **48**:53–59.

25. **Kisilevsky R, Boudreau L, Foster D**. 1983. Kinetics of amyloid deposition. II. The effects of dimethylsulfoxide and colchicine therapy. Lab Invest **48**:60–67.
26. **Kisilevsky R, Subrahmanyan L**. 1992. Serum amyloid A changes high density lipoprotein's cellular affinity. A clue to serum amyloid A's principal function. Lab Invest **66**:778–785.
27. **Kolbert KS, Watson T, Matei C, Xu S, Koutcher JA, Sgouros G.** 2003. Murine S factors for liver, spleen, and kidney. J Nucl Med **44:**784–791.
28. **Kovalchuk AL, Kim JS, Park SS, Coleman AE, Ward JM, Morse HC 3rd, Kishimoto T, Potter M, Janz S.** 2002. IL6 transgenic mouse model for extraosseous plasmacytoma. Proc Natl Acad Sci U S A **99:**1509–1514.
29. **Lindhorst E, Young D, Bagshaw W, Hyland M, Kisilevsky R.** 1997. Acute inflammation, acute phase serum amyloid A and cholesterol metabolism in the mouse. Biochim Biophys Acta **1339:**143–154.
30. **Ludlage E, Murphy CL, Davern SM, Solomon A, Weiss DT, Glenn-Smith D, Dworkin S, Mansfield KG.** 2005. Systemic AA amyloidosis in the common marmoset. Vet Pathol **42:**117–124.
31. **Madi K, De Paola D, Duarte F, Takyia C, Lima RJ.** 1990. Spontaneous amyloidosis in mice with malignant neoplasms. Exp Pathol **38:**129–134.
32. **Maita K, Hirano M, Harada T, Mitsumori K, Yoshida A, Takahashi K, Nakashima N, Kitazawa T, Enomoto A, Inui K, Shirasu Y .** 1988. Mortality, major cause of moribundity, and spontaneous tumors in CD1 mice. Toxicol Pathol **16:**340–349.
33. **Marhaug G, Dowton SB.** 1994. Serum amyloid A: an acute phase apolipoprotein and precursor of AA amyloid. Baillieres Clin Rheumatol **8:**553–573.
34. **Mensua C, Carrasco L, Bautista MJ, Biescas E, Fernandez A, Murphy CL, Weiss DT, Solomon A, Lujan L.** 2003. Pathology of AA amyloidosis in domestic sheep and goats. Vet Pathol **40:**71–80.
35. **Mezza LE, Quimby FW, Durham SK, Lewis RM.** 1984. Characterization of spontaneous amyloidosis of Syrian hamsters using the potassium permanganate method. Lab Anim Sci **34:**376–380.
36. **Papendick RE, Munson L, O'Brien TD, Johnson KH.** 1997. Systemic AA amyloidosis in captive cheetahs (Acinonyx jubatus). Vet Pathol **34:**549–556.
37. **Preciado-Patt L, Hershkoviz R, Fridkin M, Lider O.** 1996. Serum amyloid A binds specific extracellular matrix glycoproteins and induces the adhesion of resting CD4+ T cells. J Immunol **156:**1189–1195.
38. **Schell M, Wall J, Macy SD, Wooliver C, Wolfenbarger DA, Donnell R, Weiss DT, Solomon A.** Prevention of AA-amyloidosis by active immunotherapy. In: Bely M, editor. Amyloid and amyloidosis: proceedings of the IXth International Symposium on Amyloidosis. Budapest (Hungary): David Apathy.
39. **Schwick HG, Haupt H.** 1986. Properties of acute phase proteins of human plasma. Behring Inst Mitt **80:**1–10.
40. **Solomon A, Richey T, Murphy CL, Weiss DT, Wall JS, Westermark GT, Westermark P.** 2007. Amyloidogenic potential of foie gras. Proc Natl Acad Sci U S A **104:**10998–11001.
41. **Solomon A, Weiss DT, Schell M, Hrncic R, Murphy CL, Wall J, McGavin MD, Pan HJ, Kabalka GW, Paulus MJ.** 1999. Transgenic mouse model of AA amyloidosis. Am J Pathol **154:**1267–1272.
42. **Suematsu S, Matsusaka T, Matsuda T, Hirano T, Kishimoto T**. 1993. Interleukin-6 in myeloma–plasmacytoma. Int Rev Exp Pathol **34(**Pt A):91–98.
43. **Suematsu S, Matsusaka T, Matsuda T, Ohno S, Miyazaki J, Yamamura K, Hirano T, Kishimoto T.** 1992. Generation of plasmacytomas with the chromosomal translocation t(12;15) in interleukin 6 transgenic mice. Proc Natl Acad Sci USA **89:**232–235.
44. **Tam SP, Flexman A, Hulme J, Kisilevsky R.** 2002. Promoting export of macrophage cholesterol: the physiological role of a major acute-phase protein, serum amyloid A 2.1. J Lipid Res **43:**1410–1420.
45. **van der Linde-Sipman JS, Niewold TA, Tooten PC, de Neijs-Backer M, Gruys E.** 1997. Generalized AA-amyloidosis in Siamese and Oriental cats. Vet Immunol Immunopathol **56:**1–10.
46. **van Rossum M, van Asten FJ, Rofina J, Lenstra JA, Benson MD, Gruys E.** 2004. Analysis of cDNA sequences of feline SAAs. Amyloid **11:**38–43.
47. **Wall J, Schell M, Hrncic R, Macy SD, Wooliver C, Wolfenbarger DA, Murphy C, Donnell R, Weiss DT, Solomon A.** Treatment of Amyloidosis using an anti-fibril monoclonal antibody: Preclinical efficacy in a murine model of AA-amyloidosis. In: Bely M, editor. Amyloid and amyloidosis: proceedings of the IXth International Symposium on Amyloidosis. Budapest (Hungary): David Apathy.
48. **Wall JS, Kennel SJ, Paulus MJ, Gleason S, Gregor J, Baba J, Schell M, Richey T, O'Nuallain B, Donnell R, Hawkins PN, Weiss DT, Solomon A.** 2005. Quantitative high-resolution microradiographic imaging of amyloid deposits in a novel murine model of AA amyloidosis. Amyloid **12:**149–156.
49. **Wall JS, Paulus MJ, Gleason S, Gregor J, Solomon A, Kennel SJ.** 2006. Microimaging of amyloid in mice. Methods Enzymol **412:**161–182.